Retention and Permeability Properties of Damaged Porous Rocks

Jean-Michel PEREIRA[a,*], Chloé ARSON[b]

[a] *Université Paris-Est, Laboratoire Navier (UMR CNRS – IFSTTAR – ENPC), CERMES, École des Ponts ParisTech, France*
[b] *Zachry Department of Civil Engineering, Texas A&M University, USA*

Abstract

The objective of this research work is to model the influence of deformation and damage on the permeability and retention properties of cracked porous media. This is achieved thanks to the introduction of microscale information into a macroscopic damage model. To this end, the Pore Size Distribution (PSD) of the material is coupled to the mechanical behaviour of the rock. Changes to this distribution due to deformation and damage are modelled and then used to capture induced changes to the retention and permeability properties of partially saturated materials.

Rock microstructure is characterized by the Size Distributions of natural pores and cracks, which are used to update intrinsic permeability with Hagen-Poiseuille flow equation and Darcy's law. The void space occupied by water is computed by integrating the Pore Size Distributions of natural pores and cracks up to the capillary pore radius (r_{sat}). Laplace equation is used to relate r_{sat} to the capillary pressure.

*École des Ponts ParisTech, 6-8 av. B. Pascal, F–77455 Marne-la-Vallée cedex 2, FRANCE. email: jeanmichel.pereira@enpc.fr

The paper explains how to update PSD parameters with the macroscopic variables (such as deformation and damage), and then how to update permeability and retention properties with the PSD parameters. Conventional triaxial compression tests are simulated under controlled capillary pressure and under controlled water content. The proposed model captures well the intrinsic permeability decrease associated to the elastic compression of the natural pores, followed by the permeability jump due to crack opening. The modeling framework can be adapted to any rock constitutive model, including thermo-hydro-chemo-mechanical couplings. Applications may be found in energy production, ore exploitation and waste management.
Keywords: Rock, Poromechanics, Continuum Damage Mechanics, Pore Size Distribution Curve, Permeability, Retention Curve, Numerical Model, Triaxial Compression Test

1. Introduction

Multiphase flow in damaged porous media became a key topic in research related to oil and gas extraction [1, 2]. The urge to find new mineral deposits has also generated a lot of research on the influence of crystallization and dissolution processes occurring in the deep Earth crust on porosity and permeability of rock [3, 4]. Relating rock microstructure to porosity, permeability and retention properties is of prior importance in problems involving pore fluid phase changes, such as the design of deep nuclear waste disposals [5, 6] and geothermal boreholes [7, 8].

The first models based on the knowledge of the Pore Size Distribution (PSD) curve focused on unimodal porous media [9, 10]. More recent studies use the

PSD curve to determine the retention and permeability properties of bimodal porous media [11, 12, 13, 14]. However, these studies deal with undamaged materials. Following a micromechanical approach, Zhou et al. [15] introduced a penetration distance to account for crack connectivity. However, permeability is computed from a PSD curve that needs to be integrated in each possible micro-crack direction, which induces high computational costs. In dual permeability models proposed for fracture networks, flow in natural pores and cracks are governed by different equations, that may be coupled or not [16, 17, 18, 19]. In multimodal models [20], natural pores and cracks are assumed to connect and to form a unique porous network, which avoids the computation of coefficients accounting for the transfer of fluid from one network to the other. Statistical methods make it possible to account for the crack locations, lengths, apertures and orientations [21]. The main challenges in fracture network models are: the determination of equivalent flow properties at the scale of the Representative Elementary Volume [22, 23], the computation of internal length parameters, and the prediction of percolation thresholds. Moreover, most of the fracture network models do not account for the deformation of the solid skeleton nor the evolution of damage. Double porosity models overcome this limitation: for instance, Wong et al. [24] proposed to equate fluid flow from one porous network to the other as a phase change.

A few phenomenological models based on Continuum Damage Mechanics account for the effect of cracking on permeability changes. It is usually assumed that crack permeability adds to the permeability of the undamaged rock matrix [25]. In anisotropic models, the flow induced by damage is often

considered to occur in the crack planes, which makes it possible to compute crack permeability from the cubic law [26, 27]. Maleki and Pouya [28, 29] proposed a more refined approach relying on empirical percolation thresholds.

The objective of this research work is to extend the model presented in [30] to unsaturated porous rock, in order to assess the influence of deformation and damage on the permeability and retention properties of cracked porous media. The proposed approach consists in updating Pore Size Distributions (PSD) with macroscopic variables of deformation and damage. Section 2 explains how PSD parameters are related to the volume occupied by natural pores and cracks, and how to update these volume fractions with deformation and damage. Section 3 details the permeability and retention models, and presents the method to compute the intrinsic permeability, the degree of saturation and the relative permeability. Conventional triaxial compression tests have been simulated. The results obtained for tests controlled in capillary pressure are presented in Section 4, and the simulations performed at fixed water content are presented in Section 5.

2. Representation of the Damaged Microstructure

2.1. Background: Crack-Induced Porosity and Permeability in Rock

Cracks are naturally present in most rock materials [31, 32]. As a result, measuring damage requires the definition of a reference state, in which rock connected porosity is associated to a "natural" void space. In this paper, natural porosity is defined as the porosity measured before loading the sample. In the simulations presented in the sequel, the material of interest is granite

rock. Unweathered granite subjected to low pressure and low temperature gradients has a natural porosity, due to micro-cracks with a length lower than the micron. Weathered granite shows a bimodal porosity [33]: drying processes favor the penetration and crystallization of salt in the rock, which creates new void space in the range of sizes of natural pores as well as one order of magnitude higher than natural pores (Fig. 1). This gap in the pore size distribution has also been observed in clay rock damaged by mechanical stress: the typical crack length is one to two orders of magnitude larger than the average natural pore radius [28]. The main geomechanical applications of the proposed permeability model are expected to be found in excavation and geological storage problems, which involve high pressure gradients (of the order of 10 MPa or higher). According to the observations reported in the literature, the permeability model proposed in the sequel assumes that natural pores and cracks form two separate sets of pores. Each set of pores is characterized by a Pore Size Distribution (PSD). In addition, natural porosity induces some permeability, even if the latter is low (of the order of 10^{-15} m^2 in granite, for instance). Because cracks are typically one to two orders of magnitude larger (or longer) than natural pores, it is expected that cracks will intersect the connected natural porous network, even in the absence of crack coalescance. As a result, it is assumed that: (1) natural pores and cracks will form a unique, bimodal connected porous network, and (2) any occurrence of damage will enhance permeability. These two assumptions are justified by recent permeability measurements obtained by wave propagation techniques [34] (Fig. 1). However, the present model is restricted to non-interacting cracks, which explains the absence of percolation threshold in the

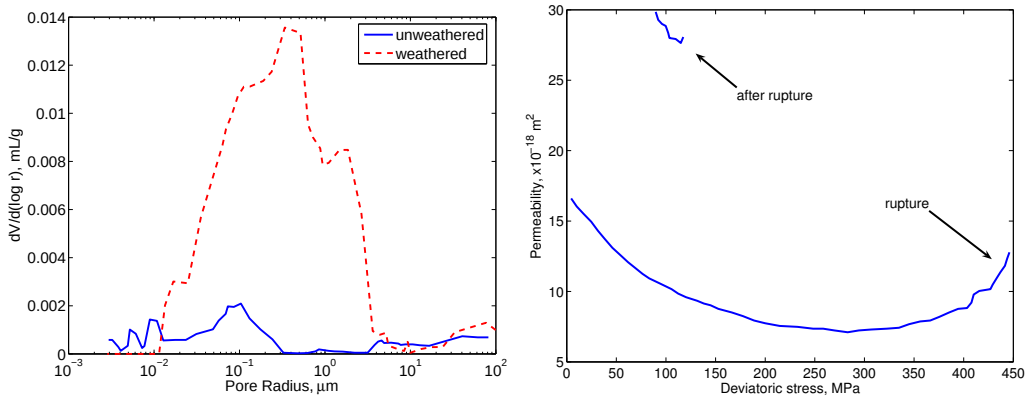

Figure 1: Damage effects on microstructure and permeability of rocks. (a) Influence of weathering damage on granite microstructure (left, modified from [33]): unimodal porosity of unweathered granite versus bimodal porosity of weathered granite. (b) Influence of damage on intrinsic permeability in saturated basalt during a triaxial compression test (right, modified from [34]).

formulation. The permeability-porosity model is based on a micro-macro coupling between natural and damage-induced porosities on the one hand, and deformation and damage variables on the other hand. The permeability model presented in this paper aims to:

1. capture crack-induced intrinsic permeability enhancement in unsaturated conditions (under control of suction and under control of water content), as it was observed in saturated conditions [34] (Fig. 1),
2. predict the trends of the evolution of the water retention curve and of the relative permeability with damage.

2.2. Relationship between Permeability and Porosity

It is assumed that natural pores and cracks do not overlap and form a unique, bimodal porous network. Natural pores and cracks in rock are

actually difficult to discriminate, even with the most advanced X-ray tomography techniques available to date [35, 36, 37**? ? ?**] Following the classical assumption used to interpret Mercury Intrusion Porosimetry data to experimentally determine PSD curves, the pores are considered as a bundle of parallel cylinders with various radii. For a unit Representative Elementary Volume (REV), the "pore size" distribution thus reduces to a "radius size" distribution. Considering that there are N_p natural pores and N_c cracks in the REV, and noting $p_p(r)$ (respectively $p_c(r)$) the probability density function of natural pores of radius r (respectively of cracks of radius r), the number of natural pores of radius r is equal to $\alpha_p(r) = N_p\, p_p(r)$, and the number of cracks of radius r is equal to $\alpha_c(r) = N_c\, p_c(r)$. For a unit REV, the pores "volume frequency" is equal to the pores "area frequency" [9]: $\alpha_p(r)\pi r^2$ for natural pores, and $\alpha_c(r)\pi r^2$ for cracks. As a result, the volume occupied by the pores in the REV can be defined as:

$$V_k \;=\; \int_{r^k_{min}}^{r^k_{max}} \alpha_k(r)\pi r^2 dr \;=\; \pi\, N_k \int_{r^k_{min}}^{r^k_{max}} p_k(r) r^2 dr, \qquad\qquad k = p,\, c \qquad (1)$$

where r^k_{min} and r^k_{max} are the minimum and maximum pore radius values ($k = p$ for natural pores, $k = c$ for cracks). It is assumed that natural pores and cracks do not overlap, but are connected. This assumption is similar to a common thought model used in homogenization theories [38], in which pores are viewed as pore spaces connected to each other by fictitious "channels" of zero volume. As a result, total porosity is the sum of pore and crack porosities, but total intrinsic permeability is not the sum of pore and crack permeabilities. Assuming that the flow in the virtual bundle of parallel cylinders is laminar, the intrinsic permeability of the damaged rock can be

computed by combining Hagen-Poiseuille flow equation to Darcy's law [9]:

$$k_{int} = \frac{\Phi}{8 \int_0^\infty f(r)dr} \int_0^\infty f(r) r^2 dr \tag{2}$$

in which Φ is the total porosity of the medium (accounting for natural pores and cracks). Assuming that all pore cuts are circles actually implies that the direction of the flow is assumed to be parallel to the direction of the pores [39]. Recalling that natural pores and cracks are assumed to connect without overlapping, and that the length of the REV in the direction of the flow is assumed to be equal to unity, the "volume frequency" $f(r)$ is equal to the "area frequency":

$$\begin{aligned} f(r) &= H(r - r^p_{min}) H(r^p_{max} - r)\, N_p\, p_p(r)\, \pi r^2 \\ &\quad + H(r - r^c_{min}) H(r^c_{max} - r)\, N_c\, p_c(r)\, \pi r^2 \end{aligned} \tag{3}$$

in which H is Heaviside function.

2.3. Relationship between Porosity and Macroscopic Variables

The macroscopic damage variable is defined as the spectral decomposition of the second-order crack density tensor [40, 41]:

$$\boldsymbol{\Omega} = \sum_{k=1}^{3} d_k\, \boldsymbol{n^k} \otimes \boldsymbol{n^k} \tag{4}$$

Total deformation is the sum of a damage-induced deformation $\boldsymbol{\epsilon^d}$ and a purely elastic deformation $\boldsymbol{\epsilon^{el}}$ (i.e. the deformation that would be obtained if the stiffness tensor were undamaged):

$$\boldsymbol{\epsilon} = \boldsymbol{\epsilon^{el}} + \boldsymbol{\epsilon^d} = \boldsymbol{\epsilon^{el}} + \boldsymbol{\epsilon^{ed}} + \boldsymbol{\epsilon^{id}} \tag{5}$$

$\boldsymbol{\epsilon}^{\boldsymbol{ed}}$ is the additional elastic deformation induced by the degradation of stiffness with cracking. Due to the existence of residual crack opening after unloading, damage not only reduces the material rigidity, but also induces irreversible strains ($\boldsymbol{\epsilon}^{\boldsymbol{id}}$) [42]. At a given state of damage, the volume occupied by the non-interactig cracks is defined as:

$$V_c \;=\; -Tr\left(\boldsymbol{\epsilon}^{\boldsymbol{ed}} + \boldsymbol{\epsilon}^{\boldsymbol{id}}\right) \;=\; -Tr\left(\boldsymbol{\epsilon}^{\boldsymbol{d}}\right) \tag{6}$$

in which the soil mechanics sign convention is used (compression counted positive). The volume occupied by natural pores is assumed to evolve with the purely elastic deformation:

$$V_p \;=\; -Tr\left(\boldsymbol{\epsilon}^{\boldsymbol{el}}\right) \tag{7}$$

The knowledge of the volume occupied by the natural pores and cracks (expressed in equation 1) makes it possible to update porosity and the "area frequency" defined in equation 3, and thus, to update the intrinsic permeability (expressed in equation 2). Natural pores and cracks volumes can be calculated at any loading step (with equations 6 and 7), as long as a constitutive model is provided to relate stress to damage and deformation. To illustrate the proposed conceptual framework, a simple mechanical damage model has been adopted in the simulations presented in the sequel: it is assumed that damage grows with tensile strains according to a common damage criterion [43, 44]:

$$f_d\left(\boldsymbol{\Omega}, \boldsymbol{\epsilon}^{+}\right) \;=\; \sqrt{\frac{1}{2}\left(g\boldsymbol{\epsilon}^{+}\right) : \left(g\boldsymbol{\epsilon}^{+}\right)} \;-\; C_0 \;-\; C_1\, \boldsymbol{\delta} : \boldsymbol{\Omega} \tag{8}$$

in which $\boldsymbol{\delta}$ is the second-order identity tensor. The parameter g relates the damage tensor to the compression stress ($\boldsymbol{\sigma}^{\boldsymbol{R}}$) that would be necessary to

close the residual cracks formed after a tensile loading followed by a bare unloading [45]: $\boldsymbol{\sigma}^{\boldsymbol{R}} = -g\,\boldsymbol{\Omega}$. C_0 is the initial damage threshold, and C_1 controls cracks growth with cumulated damage. The damage flow rule is assumed to be associated.

2.4. Updating Porous Volume Fractions with Macroscopic Variables

For a strain-controlled test, the increment of strain applied at iteration k is known. A trial increment of stress is computed, assuming that the material remains elastic during the loading iteration:

$$d\boldsymbol{\sigma}^{(k,*)} = \boldsymbol{D}\left(\boldsymbol{\Omega}^{(k-1)}\right) : d\boldsymbol{\epsilon}^{(k)} \tag{9}$$

In the mechanical damage model selected as an illustration of the conceptual framework, the damaged elasticity tensor $\boldsymbol{D}(\boldsymbol{\Omega})$ is computed by applying the Principle of Equivalent Elastic Energy (PEEE):

$$\boldsymbol{D}(\boldsymbol{\Omega}) = \boldsymbol{M}^{-1}(\boldsymbol{\Omega}) : \boldsymbol{D_0} : \boldsymbol{M}^{-T}(\boldsymbol{\Omega}) \tag{10}$$

in which $\boldsymbol{M}(\boldsymbol{\Omega})$ is the fourth-order damage operator introduced by Cordebois and Sidoroff to define effective stress $\tilde{\boldsymbol{\sigma}}$ [46]:

$$\tilde{\boldsymbol{\sigma}} = \boldsymbol{M}(\boldsymbol{\Omega}) : \boldsymbol{\sigma} = (\boldsymbol{\delta} - \boldsymbol{\Omega})^{-1/2} : \boldsymbol{\sigma} : (\boldsymbol{\delta} - \boldsymbol{\Omega})^{1/2} \tag{11}$$

in which $\boldsymbol{\delta}$ denotes the second-order identity tensor. If the undamaged material is linear elastic, with a Young's modulus E_0 and a Poisson's ratio ν_0, the damaged stiffness tensor obtained by combining Equations 10 and 11 writes,

using Voigt notations [47]:

$$\boldsymbol{D}\left(\boldsymbol{\Omega}\right) \;=\; \tfrac{E_0}{(1-2\nu_0)(1+\nu_0)}\times$$

$$\left[\begin{array}{ccc|ccc}
(1-\nu_0)(1-d_1)^2 & \nu_0(1-d_1)(1-d_2) & \nu_0(1-d_1)(1-d_3) & & & \\
\nu_0(1-d_1)(1-d_2) & (1-\nu_0)(1-d_2)^2 & \nu_0(1-d_2)(1-d_3) & & & \\
\nu_0(1-d_1)(1-d_3) & \nu_0(1-d_2)(1-d_3) & (1-\nu_0)(1-d_3)^2 & & & \\
\hline
0 & 0 & 0 & & & \\
0 & 0 & 0 & & & \\
0 & 0 & 0 & & &
\end{array}\right.$$

$$\left.\begin{array}{ccc}
0 & 0 & 0 \\
0 & 0 & 0 \\
0 & 0 & 0 \\
(1-2\nu_0)(1-d_2)(1-d_3) & 0 & 0 \\
0 & (1-2\nu_0)(1-d_1)(1-d_3) & 0 \\
0 & 0 & (1-2\nu_0)(1-d_1)(1-d_2)
\end{array}\right] \tag{12}$$

in which the d_k refer to damage eigenvalues (Eq. 4). Total strains are updated with the known incremental strains:

$$\boldsymbol{\epsilon}^{(k)} \;=\; \boldsymbol{\epsilon}^{(k-1)} + d\boldsymbol{\epsilon}^{(k)} \tag{13}$$

The sign of the damage criterion (Equation 8) is checked. If damage occurs during the iteration, the stress increment is updated as follows:

$$d\boldsymbol{\sigma} \;=\; \boldsymbol{D}\left(\boldsymbol{\Omega}\right) : d\boldsymbol{\epsilon} + \left(\frac{\partial \boldsymbol{D}\left(\boldsymbol{\Omega}\right)}{\partial \boldsymbol{\Omega}} : \boldsymbol{\epsilon}\right) : d\boldsymbol{\Omega} - d\left(\boldsymbol{D}\left(\boldsymbol{\Omega}\right) : \boldsymbol{\epsilon}^{\boldsymbol{id}}\right) \tag{14}$$

By definition of the damage-induced residual stress and residual strains $\left(\boldsymbol{\sigma}^{\boldsymbol{R}} = -g\,\boldsymbol{\Omega} = \boldsymbol{D}\left(\boldsymbol{\Omega}\right) : \boldsymbol{\epsilon}^{\boldsymbol{id}}\right)$:

$$d\boldsymbol{\sigma} = \boldsymbol{D}\left(\boldsymbol{\Omega}\right) : d\boldsymbol{\epsilon} + \left(\frac{\partial \boldsymbol{D}\left(\boldsymbol{\Omega}\right)}{\partial \boldsymbol{\Omega}} : \boldsymbol{\epsilon}\right) : d\boldsymbol{\Omega} + g d\boldsymbol{\Omega} \tag{15}$$

If damage occurs at iteration k, the stress increment is updated with the imposed strain increment as follows:

$$d\boldsymbol{\sigma}^{(k)} = \boldsymbol{D}\left(\boldsymbol{\Omega}^{(k-1)}\right) : d\boldsymbol{\epsilon}^{(k)} + \left(\frac{\partial \boldsymbol{D}\left(\boldsymbol{\Omega}^{(k-1)}\right)}{\partial \boldsymbol{\Omega}} : \boldsymbol{\epsilon}^{(k-1)}\right) : d\boldsymbol{\Omega}^{(k)} + g d\boldsymbol{\Omega}^{(k)} \tag{16}$$

After updating total strains, it is possible to get the volume of pores ($V_v = V_p + V_c$) in the REV at iteration k:

$$\boldsymbol{\epsilon}^{(k)} = \boldsymbol{\epsilon}^{(k-1)} + d\boldsymbol{\epsilon}^{(k)}, \quad {V_v}^{(k)} = -Tr\left(\boldsymbol{\epsilon}^{(k)}\right) + \Phi_0 \tag{17}$$

in which Φ_0 is the initial porosity of the rock (assumed to be initially undamaged). For any iteration, in loading or unloading conditions:

$$d\boldsymbol{\epsilon}^{el(k)} = \boldsymbol{D}\left(\boldsymbol{\Omega}^{(k-1)}\right)^{-1} : d\boldsymbol{\sigma}^{(k)} \tag{18}$$

The combination of Equations 17 and 18 gives:

$$d\boldsymbol{\epsilon}^{d(k)} = d\boldsymbol{\epsilon}^{(k)} - d\boldsymbol{\epsilon}^{el(k)}, \quad \boldsymbol{\epsilon}^{d(k)} = \boldsymbol{\epsilon}^{d(k-1)} + d\boldsymbol{\epsilon}^{d(k)} \tag{19}$$

from which it is possible to update the volume fractions of cracks and natural pores (Equations 6 and 7):

$${V_c}^{(k)} = -Tr\left(\boldsymbol{\epsilon}^{d(k)}\right), \quad {V_p}^{(k)} = {V_v}^{(k)} - {V_c}^{(k)} \tag{20}$$

3. Computation of Permeability and Degree of Saturation

3.1. Constitutive Model

When the porous network is filled with two fluids, the non-wetting fluid is defined as the one that has a contact angle (θ_{nw}) greater than 90^o, and the wetting fluid is defined as the fluid that has a contact angle (θ_w) less than 90^o. Capillary pressure (p_c) is defined as the difference between the pressure of the non-wetting fluid (p_{nw}) and the pressure of the wetting fluid (p_w), and is related to the capillary pore radius (r_{sat}) by the Washburn-Laplace equation [9, 11]:

$$p_c = p_{nw} - p_w = \frac{2\sigma_{nw/w} cos\theta_w}{r_{sat}} \tag{21}$$

in which $\sigma_{nw/w}$ is the surface tension in the meniscus separating the two fluid phases. In many approaches [9, 11], it is assumed that the tubes constituting the porous network are either saturated with the wetting fluid, or completely filled with the non-wetting fluid. With this assumption, equation 21 may be interpreted as follows:

- for $r > r_{sat}$, $p_c(r) < p_c$, i.e. the capillary pressure p_c is higher than the capillary pressure ensuring the equilibrium of the meniscus, so the tube is filled with the non-wetting fluid,

- for $r < r_{sat}$, $p_c(r) > p_c$, i.e. the capillary pressure p_c is lower than the capillary pressure ensuring the equilibrium of the meniscus, so the tube is filled with the wetting fluid.

In the present approach, according to the postulate of local state, any evolution is considered as the succession of incremental evolutions between two

equilibrium states. This amounts to say that transient effects associated to drying/wetting processes are neglected. To model the time history of the saturation process, a more refined representation of the microstructure would be needed. Blunt et al. studied the evolution of the capillary fringe by making a distinction between pores and throats [48, 49]. In order to account for the presence of residual films of the wetting phase during draining paths, Blunt proposed to model the porous space as a network of cylinders of triangular section [50]. Wettability variations can be accounted for due to the presence of corners in the shape of the pores cross section. In its current development, the proposed model assumes that pores are circular cylinders, and saturation history is not accounted for. If the current capillary pressure is known, it is thus possible to determine the value of the pore radius satisfying equation 21 (noted r_{sat}). Without loosing the general validity of the presented framework, the wetting fluid is assumed to be liquid water, and the non-wetting fluid is assumed to be gaseous air. The volume of water in the REV (V_w) is equal to the volume of the pores that have a radius lower than r_{sat}. As a result, V_w is obtained by restricting the integral of the volume frequencies (equation 1) to the appropriate interval. At this point, it is essential to figure out in which family of pores (either natural or cracks) r_{sat} is located. Since it is assumed that these families do not overlap (i.e. $r^p_{max} < r^c_{min}$), V_w is simply obtained by:

$$V_w = \int_{r^p_{min}}^{r_{sat}} H(r_{sat} - r^p_{min}) H(r^p_{max} - r_{sat}) \alpha_p(r) \pi r^2 dr \tag{22}$$

if $r_{sat} \in [r^p_{min}, r^p_{max}]$ and by:

$$V_w = V_p + \int_{r^c_{min}}^{r_{sat}} H(r_{sat} - r^c_{min}) H(r^c_{max} - r_{sat}) \alpha_c(r) \pi r^2 dr \tag{23}$$

if $r_{sat} \in [r^c_{min}, r^c_{max}]$. The degree of saturation is defined as:

$$S_w = \frac{V_w}{V_p + V_c} \tag{24}$$

Noting V_{REV} the Representative Elementary Volume, we have: $V_v = \int_0^\infty f(r)dr$ and $\Phi = V_v/V_{REV}$. As a result, combining equations 1, 2 and 3 provides the expression of the damaged intrinsic rock permeability:

$$k_{int} = \frac{1}{8\,V_{REV}} \left(\int_{r^p_{min}}^{r^p_{max}} \alpha_p(r)\pi r^4 dr + \int_{r^c_{min}}^{r^c_{max}} \alpha_c(r)\pi r^4 dr \right) \tag{25}$$

The total (or apparent) permeability of the damaged unsaturated can be expressed in the same way as:

$$k_w = \frac{1}{8\,V_{REV}} \int_{r^p_{min}}^{r_{sat}} H(r_{sat} - r^p_{min}) H(r^p_{max} - r_{sat}) \alpha_p(r)\pi r^4 dr \tag{26}$$

if $r_{sat} \in [r^p_{min}, r^p_{max}]$ and as:

$$\begin{aligned} k_w \;=\; & \tfrac{1}{8\,V_{REV}} \textstyle\int_{r^p_{min}}^{r^p_{max}} H(r_{sat} - r^p_{min}) H(r^p_{max} - r_{sat}) \alpha_p(r)\pi r^4 dr \\ & + \tfrac{1}{8\,V_{REV}} \textstyle\int_{r^c_{min}}^{r_{sat}} H(r_{sat} - r^c_{min}) H(r^c_{max} - r_{sat}) \alpha_c(r)\pi r^4 dr \end{aligned} \tag{27}$$

if $r_{sat} \in [r^c_{min}, r^c_{max}]$. The relative permeability k_R can then be obtained using the following relation:

$$k_R = k_w / k_{int} \tag{28}$$

3.2. Computational Algorithm

The computational algorithm to update permeability and retention properties with macroscopic variables is summarized below. Interested readers are referred to [30] for a detailed version of the algorithm related to the damage and its effects on permeability of saturated rocks.

1. The main steps to update the volume fractions of natural pores and cracks in a strain-controlled test are indicated in Subsection 2.4.
2. Once V_p and V_c are known, it is possible to update the parameters of the probability functions $p_p(r)$ and $p_c(r)$. In the simulations presented in the sequel, the radius size of natural pores follows a Gauss distribution [10], and the radius size of cracks follows an exponential distribution [28]. Crack length (λ_c) is the only parameter of the exponential distribution $p_c(r)$. λ_c is assumed to be a fixed parameter of the model, and is computed by using the mathematical definition of the mean value of a random variable. The number of cracks in the Representative Elementary Volume (N_c) is then updated with V_c (equation 1). Given the initial void ratio, it is also possible to use definitions of the theory of probabilities in order to compute the initial number of natural pores (N_p^0), the initial standard deviation (s^0) and the initial mean value of the natural pores (m^0). After the initial stage, N_p and s are considered fixed parameters of the model and the mean radius of natural pores is updated with V_p (equation 1). In practice, the value of the standard deviation used in the resolution algorithm was fixed to one third of the range of values $[r_p^{min}, r_p^{max}]$. The model parameters were post-processed for various choices of $s = s^0$ to verify that the simulation results presented in the following were not sensitive to the choice of s^0 for the pore sizes considered.
3. Once the parameters of the probability density functions have been updated with the macroscopic variables, it is possible to update the intrinsic permeability according to equation 25.

4. The final step consists in determining r_{sat}.

   - If the test is performed with a control of capillary pressure, r_{sat} is computed by using Laplace equation (equation 21). For water, we have [51]: $\sigma_{nw/w} = 72.75\,10^{-3}$ N/m and $\cos\theta_w = 1$ (assuming a null contact angle between water and solid). The degree of saturation is updated by using equation 22 or 23 and equation 24, and the relative permeability is computed by combining equation 25 and equation 26 or 27.

   - The procedure differs slightly if the test is performed with a control of water content. First recall that water content (w) is defined as the ratio of the mass of water by the mass of solid grains contained in the sample: $w = M_w/M_s$. Noting e the void ratio of the sample, and G_s the specific gravity of the solid phase, we have [52]:

$$e\,S_w \;=\; w\,G_s \tag{29}$$

     G_s is a constant, and w is assumed to be fixed. Assuming that the initial porosity is given, the volume occupied by the voids is known at this stage of the computations (equation 17). The solid phase is considered incompressible, so that the volume occupied by the solid grains at the current iteration is equal to the volume occupied by the solid phase in the initial state: $V_s = 1 - \Phi_0$ for a unit initial REV. It is thus possible to determine the void ratio and the degree of saturation at the current iteration:

$$e^{(k)} \;=\; \frac{V_v^{(k)}}{V_s}, \qquad\qquad S_w^{(k)} \;=\; \frac{w\,G_s}{e^{(k)}} \tag{30}$$

At high pressures, the assumption of incompressible solid grains may be unrealistic. The proposed modeling framework can easily be extended to compressible grains by means of Biot coefficients [53]. The latter do depend on damage, but this dependence actually exists due to the dependence of Biot's coefficients on the damaged stiffness tensor, the expression of which is already derived from principles of Continuum Damage Mechanics in the present modeling framework. Combining relations 30, 24 and 22 or 23 provides an equation that can be solved for r_{sat}. The capillary pressure can be obtained by Laplace equation (equation 21) in order to determine the retention curve at any stage of damage. The relative permeability is updated by using equation 25 and equation 26 or 27.

It has to be noted that among the nine microscopic parameters involved in the model formulation (r^p_{min}, r^p_{max}, r^c_{min}, r^c_{max}, N_p, N_c, m, s and λ_c):

1. the average size of the natural pores (m) and the number of cracks developed in the REV (N_c) are updated with macroscopic variables (e.g., deformation and damage),
2. the number of natural pores (N_p), the standard deviation of the natural pore size distribution (s) and the crack length (λ_c) are deduced from definitions used in the theory of probability,
3. only the ranges of values of the natural pores and cracks (r^p_{min}, r^p_{max}, r^c_{min} and r^c_{max}) are fixed parameters that need to be provided by the user.

The minimum and maximum void sizes observed at a certain state of damage (and in the undamaged configuration in particular) do change as deformation and damage evolve: for instance, the longest crack observed at 10% damage is likely to be shorter than the longest crack observed for 50% damage. The bounds indicated as model parameters herein embrace all the possible values that can be taken by the natural pores and cracks, i.e. for all the states of deformation and damage of the rock before failure. It is understated that the values of pore sizes close to the bounds are "improbable events" in the sense of mathematics (i.e., events with a zero probability of occurrence). The parameters controlling the shape of the PSDs (mainly: N_p, N_c, m, s and λ_c) are thus assumed to be sufficient to capture the main pore size changes induced by deformation and damage. As a result, the size that separates pores from cracks is considered as a material parameter. The authors reckon that this is an idealized assumption. However, updating the bounds of pore radii ranges of values would require an update of the size of the Representative Elementary Volume, which constitutes an area of research per se [54].

4. Permeability and Retention Properties with Control of Capillary Pressure

A conventional triaxial compression test is simulated, by increasing ϵ_1 by increments while maintaining a constant confinement (radial stress is constant, equal to 100 MPa). Capillary pressure is fixed throughout the test (two tests are simulated, the first at a capillary pressure of 100 kPa and the second at 300 kPa). The material under study is a granite for which experimental results on drained triaxial compression tests have already been

Table 1: Main material parameters used to simulate unconfined triaxial compression tests on Vienne Granite.

E_0(Pa)	ν_0 (-)	g (Pa)	C_0 (Pa)	C_1 (Pa)	e_0 (-)
$8.01e10$	0.28	$-3.3e8$	$1.1e5$	$2.2e6$	0.008

r^p_{min} (μm)	r^p_{max} (μm)	r^c_{min} (μm)	r^c_{max} (μm)
0.01	1	1	10

published [55]. The mechanical damage model presented in Subsection 2.4 has proved to reproduce well the semi-brittle behavior of this granite [56, 57]. The mechanical parameters (E_0, ν_0, g, C_0, C_1) are taken equal to the ones that are calibrated in [56, 57]. The initial void ratio (e_0) is taken equal to the void ratio measured on Vienne granite [55], which is the rock studied in the calibration presented in [56, 57]. The minimum and maximum radii of the granite natural pores (r^p_{min} and r^p_{max}) are chosen so that the mean of r_p can be expected to be of the order of 0.1μm, as stated in [33]. The orders of magnitude for the minimum and maximum radii of the cracks (r^c_{min} and r^c_{max}) are chosen according to Maleki [28], who also worked on damage in rock materials. The main material parameters are summarized in Table 1.

Figure 2 presents the deviatoric stress and damage variable as functions of the imposed axial strain. The first stage corresponding to the isotropic compression from 0 to 100 MPa is also plotted. As already shown in previous studies, damage occurs when shear strains start to increase. The apparent

stiffness degrades as damage is produced and the deviatoric stress presents a significant drop after having reached a peak. This strain level corresponds to the predicted failure of the sample. It is worth noting that damage does not depend on the material hydraulic behavior (equation 8). As a result, the stress/strain curves obtained for both controlled capillary pressure tests are strictly identical.

Figure 3 highlights the evolution of the volumetric fractions of voids (V_v), natural pores (V_p) and cracks (V_c), as functions of the imposed axial deformation. Before occurrence of any damage, the evolution of the volume of voids (which is directly related to the porosity changes if the solid phase is assumed incompressible) is solely due to changes of the volume of natural pores. The volumetric behavior is contractant. As soon as cracks start to appear, the decrease of the voids volume starts to slow down, and eventually the sample's volume starts to expand. The final rebound of the natural pores' volume is due to the stress release after the stress peak.

One of the main strengths of the present model is to relate macroscopic deformation to changes of the pore size distribution of the material. As a consequence, the deformation of the natural porous network and the occurrence of cracking due to damage can clearly be observed in Figure 4, in terms of PSD curve and cumulated porosity with pores radius. It shows the PSD of the intact sample (continuous line - before loading) and of the damage sample at the end of the deviatoric compression (dashed line). As expected, the damaged material presents a bi-modal curve. Again, these PSD and cumulated porosity curves are strictly identical whatever the imposed capillary pressure because of the coupling assumptions. The values of the radii

corresponding to the two imposed pressures (through Laplace law) are also shown. It can clearly be seen that the imposed capillary pressure of 300 kPa corresponds to a radius (denoted r_{300} in the figure) belonging to the natural porous network. Inversely, for the other test, the capillary pressure of 100 kPa (denoted r_{100}) corresponds to a radius higher than the maximum radius of natural pores, and is located within the range of radii of developing cracks.

The knowledge of the evolution of the PSD enables the calculation of the evolution of the retention properties and of the saturation state of the material. In Figure 5, the water retention curves of the material are plotted at three different stages of the test (initial (A), intermediate stage corresponding to the maximum value of the degree of saturation (B) and final stage (C)). It can be seen that at low degrees of saturation, the curve is shifted upwards during the test. This means that for a given capillary pressure, the volumetric fraction of voids saturated with the wetting phase tends to increase. This corresponds to the compression of the smallest pores (natural network). Simultaneously, developing cracks form additional void space made of large pores, that are easier to desaturate because cracks are characterised by higher air entry radii. This explains why the part of the retention curve defined for high degrees of saturation is ultimately shifted downwards during the test. Figure 6 shows the evolution of the degree of saturation during the tests performed at constant capillary pressures of 100 and 300 kPa. It can be seen that for the test performed at the lowest pressure the material starts at a saturated state (capillary pressure below the air entry value of the rock) and becomes partially saturated when cracks open. A peak of degree

of saturation (at which the water retention curve denoted B in Figure 5 is plotted) is observed for the second test. It corresponds to the lowest porosity during the test.

The effects of deformation and damage of the material on the apparent and intrinsic permeabilities can be caught through changes of the PSD curve. This point is illustrated in Figure 7 which plots the evolutions of apparent, intrinsic (top) and relative (bottom) permeabilities as a function of the axial deformation (left) and damage variable (right). Intrinsic permeability (continuous lines of top sub-figures) decreases when the sample volume decreases and increases when damage becomes significant because the cracks tend to facilitate fluid flow. Interestingly enough, the apparent permeability (dash-dotted lines in top sub-figures) remains almost constant so that the relative permeability present a trend which is totally the inverse of that of the intrinsic permeability. In these tests, the total amount of water remains located within the smallest natural pores and the contribution of these pores to the water flow is not much affected by the deformation of the natural pores network.

The permeability trends predicted by the model are now compared to classical permeability models. Figure 8 shows the evolution of the intrinsic permeability (normalised by the value at the initial state) with porosity, as predicted by the present model and by Kozeny-Carman model [58, 59]. The initial stage of the test, where porosity changes are dominated by compressive deformation, follows reasonably well Kozeny-Carman equation. As soon as damage occurs and porosity bounces back, the present simulations show an increase of intrinsic permeability, corresponding to the growth of

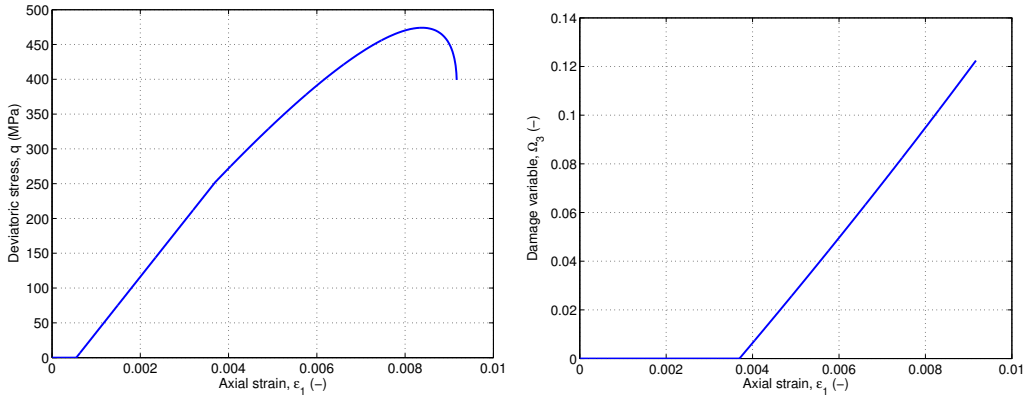

Figure 2: Stress/strain curve (left) and damage variable (right) during triaxial compression at constant capillary pressure $p_c = 100$ kPa.

the volumetric fraction of voids. Kozeny-Carman model cannot capture the difference between the initial elastic pore compression and the subsequent non-elastic pore creations related to the formation of cracks. As a result, the crack-induced porosity increase is considered as an elastic expansion of the volume of voids. The increase of permeability predicted by Kozeny-Carman model follows the same path as the decrease of permeability due to elastic compression (reversible path). It is worth noting that the trend predicted by the proposed model is consistent with the experimental observations reported in Figure 1 contrary to predictions based on Kozeny-Carman model.

Relative permeability evolution is compared to simple functions of the degree of saturation (power laws). It can be observed that a satisfactory fitting is observed (for both exponents 2 and 3 considered) when damage is null or small and that the trends diverge when damage becomes significant. This could be expected, since power laws have initially been proposed to model retention properties in unimodal porous networks.

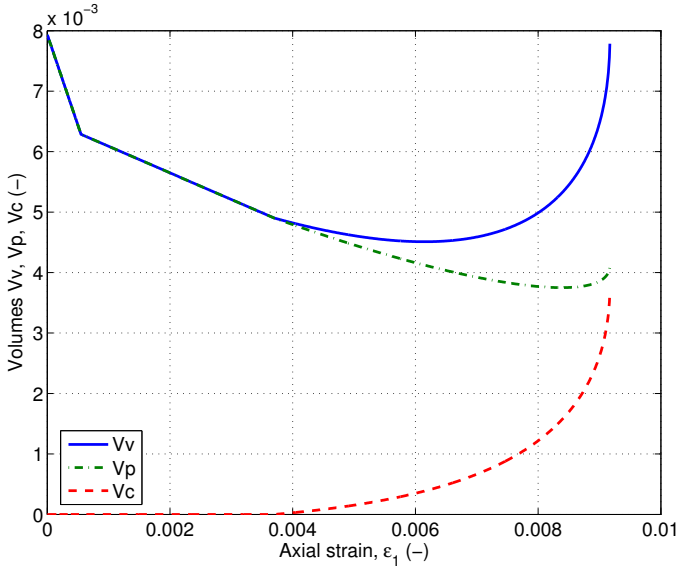

Figure 3: Evolution of volumes V_v, V_p and V_c during triaxial compression at constant capillary pressure $p_c = 100$ kPa.

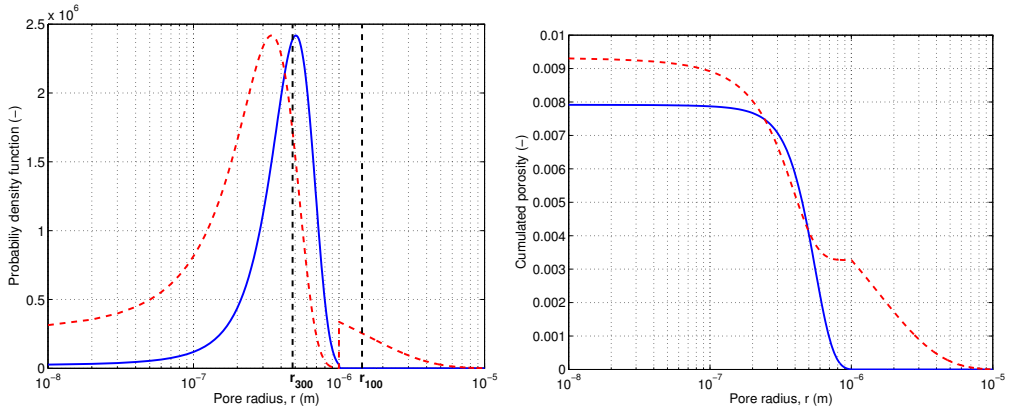

Figure 4: (Left) PSD curves (left) and cumulated porosity (right) vs pore radius of original (continuous line) and damaged (dashed-line) material during triaxial compression at constant capillary pressure. r_{100} (resp. r_{300}) denotes the value of the pore radius below which pores are saturated under a capillary pressure of $p_c = 100kPa$ (resp. $p_c = 300kPa$).

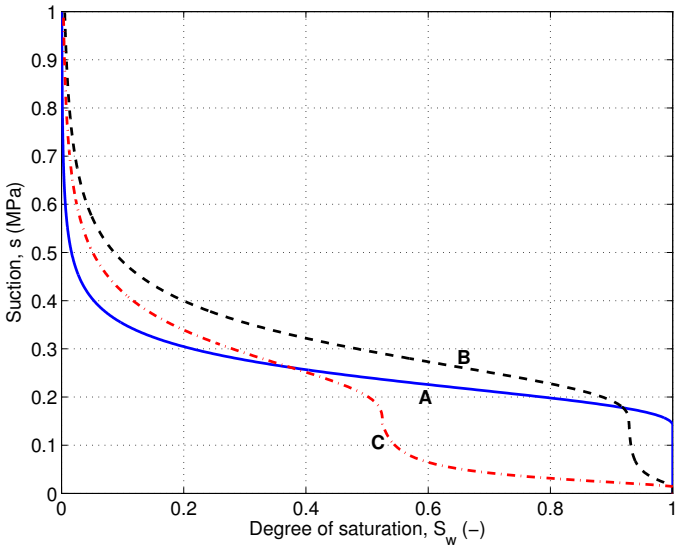

Figure 5: Water retention curves of the rock during the triaxial compression test under a constant capillary pressure of $p_c = 300$ kPa: initial state (A), damaged state with maximum degree of saturation (B), final state (C).

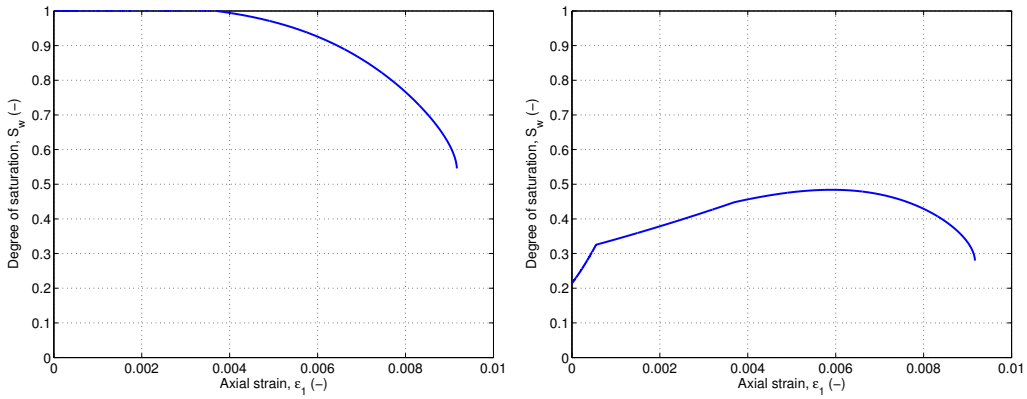

Figure 6: Evolution of degree of saturation during triaxial compression at constant capillary pressure: $p_c = 100$ kPa (left) and $p_c = 300$ kPa (right).

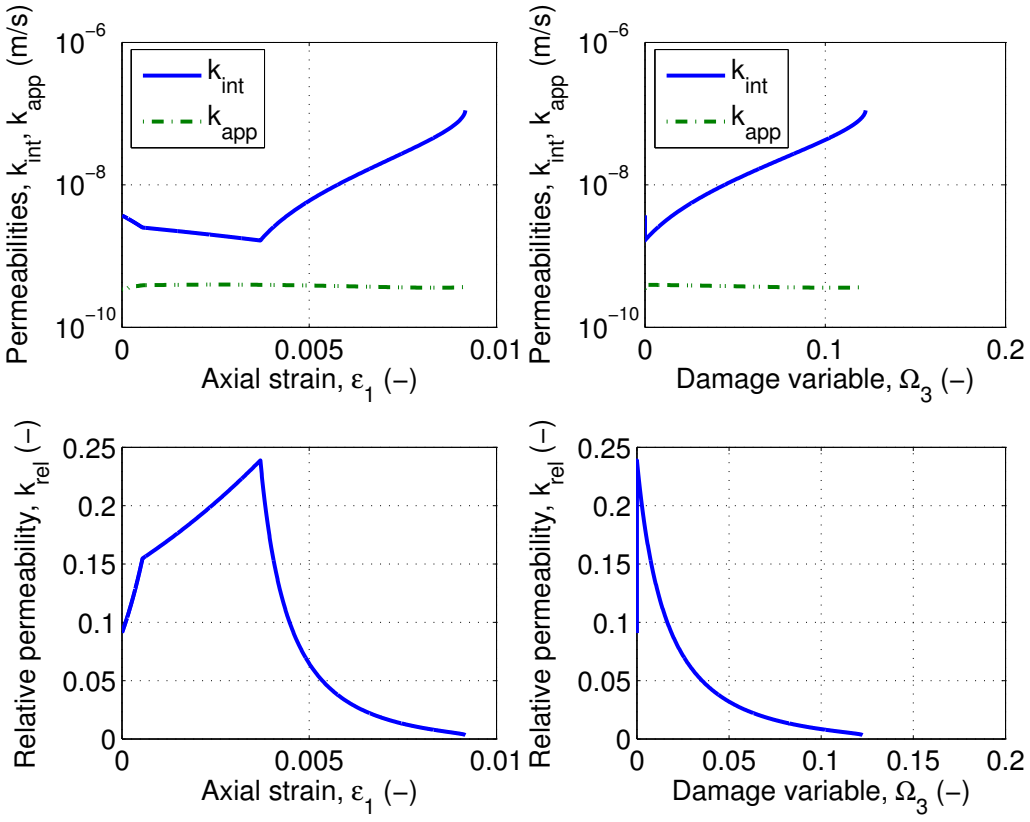

Figure 7: Evolution of total, intrinsic and relative permeabilities versus axial deformation (left) or damage variable (right) during triaxial compression at constant capillary pressure $p_c = 300$ kPa.

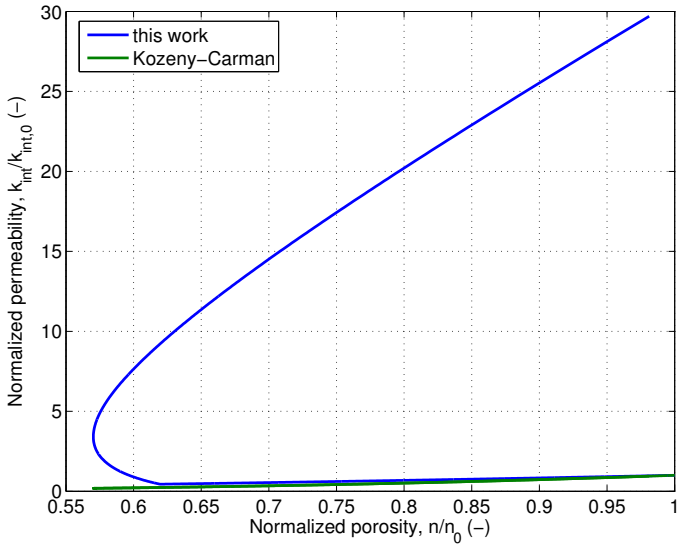

Figure 8: Evolution of the intrinsic permeability versus porosity during triaxial compression at constant capillary pressure $p_c = 100$ kPa.

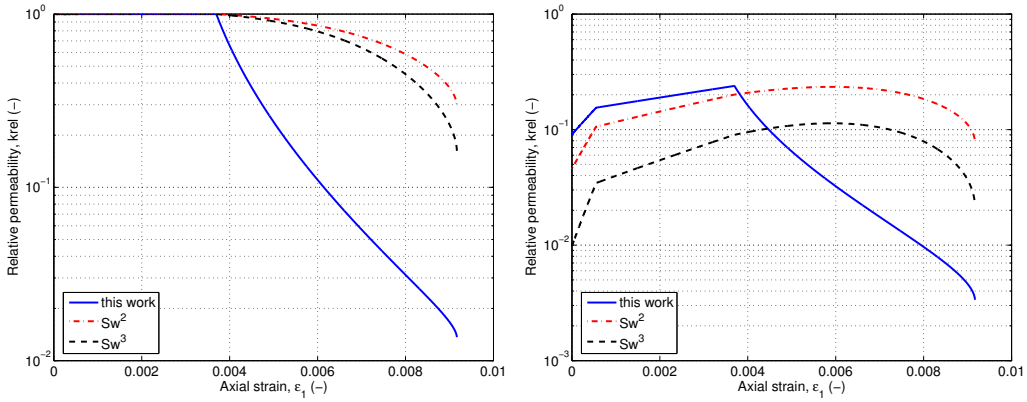

Figure 9: Evolution of the relative permeability during triaxial compression at constant capillary pressure: $p_c = 100$ kPa (left) and $p_c = 300$ kPa (right).

5. Permeability and Retention Properties with Control of Water Content

Two compression tests followed by a conventional triaxial compression are now simulated for fixed values of the water content, for the same rock material (Table 1). These two tests correspond to water contents that are in equilibrium at the initial state with capillary pressures (denoted $p_{c,0}$) of 300 kPa and 500 kPa, respectively.

Figure 10 shows the evolution of the degree of saturation together with that of the capillary pressure (or suction) for the two compression tests. As in controlled suction tests and according to equation 29, the degree of saturation first increases (due to the decrease of the void ratio, dominated by elastic compression), and then decreases rapidly (due to the growth of the void space related to crack opening). In both cases, suction increases throughout the whole test. Initially, when the degree of saturation increases, the limit size of the saturated pores (r_{sat}) is located in the natural pores. Natural pore shrinkage due to elastic compression reduces r_{sat}, which corresponds to a capillary pressure increase according to equation 21. In the second stage, the degree of saturation decreases because of the creation of new void space in developing cracks.

Figure 11 shows the evolution of the relative permeability during the two tests. A comparison with the trends given by the power laws used previously is performed. It can be observed that the predictions given by the present model, based on a microscopic approach, differ from the unimodal models of relative permeability. The differences are larger than in the previous suction-controlled tests, and are more important for high values of damage. This

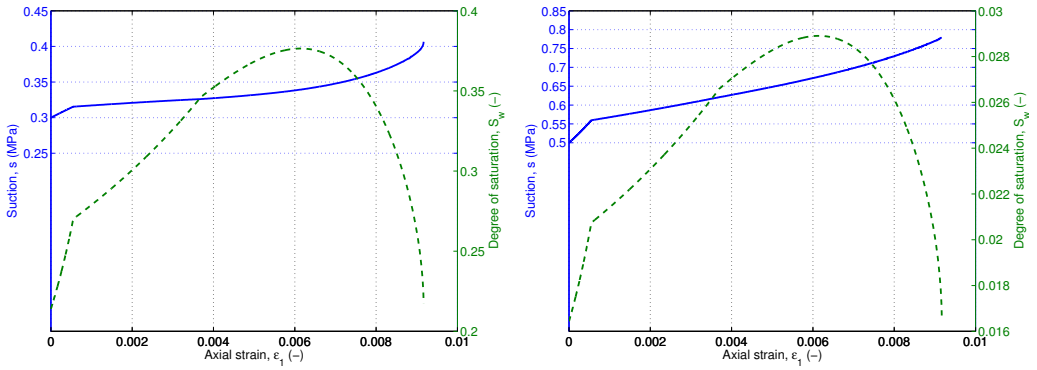

Figure 10: Evolution of suction and degree of saturation during triaxial compression at constant water content ($p_{c,0} = 300$ kPa (left) and $p_{c,0} = 500$ kPa (right)).

demonstrates the ability of the proposed model to capture microstructure changes. As explained before, suction variations are sensitive to the radius size distributions and to the limit size of saturated pores (r_{sat}). The tests performed at constant water content involve higher suctions than in the tests performed at constant capillary pressure, which emphasizes the difference between the current model predictions and classical power laws.

6. Conclusion

A permeability model is proposed for unsaturated cracked porous media. In all the tests simulated in the paper, the Representative Elementary Volume is assumed to be undamaged in the initial state. Initial porosity is associated to "natural pores" created before loading. Rock microstructure is characterized by the Size Distributions of natural pores and cracks. The volume occupied by the cracks is updated with damage-induced elastic and inelastic strains, whereas the volume occupied by natural pores is updated with purely elastic deformation. The conceptual model is general, and can be adapted to

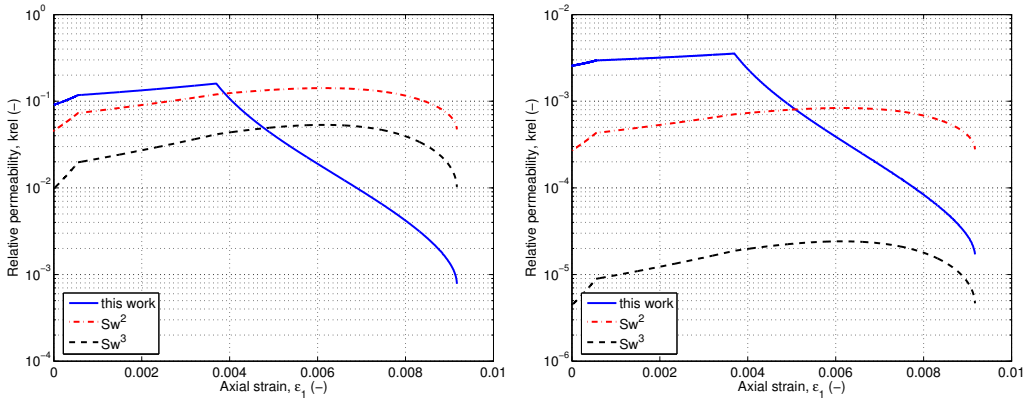

Figure 11: Evolution of relative permeability during triaxial compression at constant water content ($p_{c,0} = 300$ kPa (left) and $p_{c,0} = 500$ kPa, (right)).

any damage constitutive model providing the evolution of damage-induced deformation. The intrinsic permeability of the damaged rock is updated with the volume fractions of natural pores and cracks, by using Hagen-Poiseuille flow equation and Darcy's law. The void space occupied by water is computed by integrating the Pore Size Distributions (PSD) of natural pores and cracks up to the capillary pore radius (r_{sat}). The latter defines the size below which pores are saturated with water, and above which pores are saturated with air. Laplace equation is used to relate r_{sat} to the capillary pressure. The paper explains how to update PSD parameters with deformation and damage macroscopic variables, and then how to update the permeability and retention properties with the PSD parameters. The main original contributions of the presented work are the prediction of the evolution of bimodal PSD curves with crack propagation, and the relationship between deformation and damage on the one hand and water retention curve and apparent permeability on the other hand. Unconfined triaxial compression tests are simulated un-

der controlled capillary pressure and under controlled water content. The proposed model captures well the intrinsic permeability decrease associated to the elastic compression of the natural pores, followed by the permeability jump due to crack opening. The PSD curves evolve with the deformation and damage of the material. Obtained results catch the main features observed in laboratory tests, such as: (1) the decrease of the characteristic size of natural pores because of compression, and (2) the creation of much larger pores corresponding to the damage-induced cracks. The model can also predict changes in the relative permeability during tests on partially saturated materials. In particular, the model predicts that the apparent permeability of the sample remains constant throughout a compression test performed at constant capillary pressure, and that the suction keeps increasing in a compression test performed at constant water content.

The proposed model requires a limited number of microscopic parameters, which can easily be determined in the laboratory by Mercury Intrusion Tests (for the PSD parameters) and by microscope observations (for the minimum and maximum pore and crack sizes). The modeling framework can be adapted to any rock constitutive model, including thermo-hydro-chemo-mechanical couplings, and for problems related to damage or not. In particular, the effects of thermal expansion and chemical dissolution on rock microstructure and porosity can be accounted for, as long as the appropriate state equations and evolution functions are provided. The key issue consists in splitting deformation in order to relate strain components to PSD integrals. The approach is expected to facilitate multi-phase fluid flow predictions in cracked porous media. Potential applications may be found in

energy production, ore exploitation and waste management.

References

[1] D. Bourdet, Well Test Analysis: the use of advanced interpretation models, Elsevier, Amsterdam, The Netherlands, 2002.

[2] M. Honarpour, L. Koederitz, A. Harvey, Relative permeability of petroleum reservoirs, CRC Press, Inc. Boca Raton, Florida, 1986.

[3] C. Zhao, B. Hobbs, A. Ord, Convective and Advective Heat Transfer in Geological Systems, Springer, Berlin, 2008.

[4] C. Zhao, B. Hobbs, A. Ord, Fundamentals of Computational Geoscience: Numerical Methods and Algorithms, Springer, Berlin, 2009.

[5] A. Gens, A. Garcia-Molina, S. Olivella, E. Alonso, F. Huertas, Analysis of a full scale in situ test simulating repository conditions, International Journal for Numerical and Analytical Methods in Geomechanics 22 (1998) 515–548.

[6] C. Tsang, F. Bernier, C. Davies, Geohydromechanical processes in the excavation damaged zone in crystalline rock, rock salt, and indurated and plastic clays - in the context of radioactive waste disposal, International Journal of Rock Mechanics and Mining Sciences 42 (2005) 109–125.

[7] H. Brandl, Energy foundations and other thermo-active ground structures, Géotechnique 56 (2006) 81–122.

[8] J. Lund, Characteristics, development and utilization of geothermal resources, Geo-Heat Center Bulletin 28 (2) (2007) 1–9.

[9] I. Garcia-Bengoechea, C. Lowell, A. Altschaeffl, Pore distribution and permeability of silty clays, J. Geotech. Eng. Div. 105 (1979) 839–856.

[10] M. VanGenuchten, A closed-form equation for predicting the hydraulic conductivity of unsaturated soils, Soil Science Society of America Journal 44 (1980) 892–898.

[11] E. Romero, Characterisation and thermo-hydro-mechanical behavior of unsaturated boom clay: an experimental study, Ph.D. thesis, Univertitat Politecnica de Catalunya, Barcelona (1999).

[12] E. Rojas, G. Gallegos, J. Leal, A porous model based on porosimetry to simulate retention curves, in: E. E. Alonso, A. Gens (Eds.), Unsaturated Soils - Proc. of the 5th Int. Conf. on Unsaturated Soils, Vol. 2, CRC Press, Barcelona, Spain, 2011, pp. 927–932.

[13] A. Russell, Water retention characteristics of soils with double porosity, European Journal of Soil Science 61 (2010) 412–424.

[14] R. Salgueiro, S. Olivella, J. Suriol, Constitutive model developments for compacted unsaturated fine grained soils based on porosimetry, in: E. E. Alonso, A. Gens (Eds.), Unsaturated Soils - Proc. of the 5th Int. Conf. on Unsaturated Soils, Vol. 2, CRC Press, Barcelona, Spain, 2011, pp. 951–956.

[15] H. Zhou, J. Shao, X. Feng, D. Hu, Coupling analysis between stress

induced anisotropic damage and permeability variation in brittle rocks, Key Engineering Materials 340-341 (2007) 1133–1138.

[16] H. Gerke, M. VanGenuchten, A dual-porosity model for simulating the preferential movement of water and solutes in structured porous media, Water Resources Research 29 (1993) 305–319.

[17] J. Gwo, P. Jardine, G. Wilson, G. Yeh, A multiple-pore-region concept to modeling mass transfer in subsurface media, J. Hydrol. 164 (1995) 217–237.

[18] T. Vogel, H. Gerke, R. Zhang, M. V. Genuchten, Modeling flow and transport in a two-dimensional dual-permeability system with spatially variable hydraulic properties, J. Hydrol. 238 (2000) 78–89.

[19] R. Zimmerman, T. Hagdu, G. Bodvarsson, A new lumped-parameter model for flow in unsaturated dual-porosity media, Adv. Water Resour. 19 (1996) 317–327.

[20] W. Durner, Hydraulic conductivity estimation for soils with heterogeneous pore structure, Water Resour. Res. 30 (2) (1994) 211–223.

[21] J. Long, J. Remer, C. Wilson, P. Witherspoon, Porous media equivalents for networks of discontinuous fractures, Water Resources Research 18 (3) (1982) 645–658.

[22] R. Peters, E. Klavetter, A continuum model for water movement in an unsaturated fractured rock mass, Water Resources Research 24 (1988) 416–430.

[23] K. Pruess, J. Wang, Y. Tsang, On thermohydrologic conditions near high-level nuclear wastes emplaced in partially saturated fractured tuff. 2. effective continuum approximation., Water Resour. Res. 26 (1990) 1249–1261.

[24] H. Wong, C. Leo, J.-M. Pereira, P. Dubujet, Sedimentation-consolidation of a double porosity material, Computers and Geotechnics 34 (2007) 532–538.

[25] K. Chan, S. Bodner, D. Munson, Permeability of wipp salt during damage evolution and healing, International Journal of Damage Mechanics 10 (2001) 347–375.

[26] J. Shao, H. Zhou, K. Chau, Coupling between anisotropic damage and permeability variation in brittle rocks, International Journal for Numerical and Analytical Methods in Geomechanics 29 (2005) 12311247.

[27] J. Zhou, J. Shao, Xu, Coupled modeling of damage growth and permeability variation in brittle rocks, Mechanics Research Communications 33 (2006) 450–459.

[28] K. Maleki, Modélisation numérique du couplage entre l'endommagement et la perméabilité des roches - application à l'étude des ouvrages de stockage souterrain, Ph.D. thesis, Ecole Nationale des Ponts et Chaussées (2004).

[29] K. Maleki, A. Pouya, Numerical simulation of damage-permeability relationship in brittle geomaterials, Computers and Geotechnics 37 (2004) 619–628.

[30] C. Arson, J.-M. Pereira, Influence of damage on pore size distribution and permeability of rocks, International Journal for Numerical and Analytical Methods in Geomechanics (2012) DOI: 10.1002/nag.1123.

[31] R. Goodman, Introduction to Rock Mechanics, Second edition, Wiley, 1989.

[32] J. Jaeger, N. Cook, R. Zimmerman, Fundamentals of rock Mechanics, Fourth edition, Blackwell Publishing, 2007.

[33] C. Alves, M. S. Braga, C. Hammecker, Water transfer and decay of granitic stones in monuments, C.R. Acad. Sci. Paris, serie IIa (Surface Geosciences) (1996) 397–402.

[34] J. Fortin, S. Stanchits, S. Vinciguerra, Y. Guéguen, Influence of thermal and mechanical cracks on permeability and elastic wave velocities in a basalt from mt. etna volcano subjected to elevated pressure, Tectonophysics 503 (2011) 60–74.

[35] A. Byrnes, Reservoir characteristics of low-permeability sandstones in the rocky mountains, The Mountain Geologist 34 (1997) 39–51.

[36] Y. Ghorbani, M. Becker, J. Petersen, S. Morar, A. Mainza, J.-P. Franzidis, Use of x-ray computed tomography to investigate crack distribution and mineral dissemination in sphalerite ore particles, Minerals Engineering 24 (2011) 1249–1257.

[37] F. Renard, D. Bernard, J. Desrues, A. Ougier-Simonin, 3d imaging of fracture propagation using synchrotron x-ray microtomography, Earth and Planetary Science Letters 286 (2009) 285291.

[38] L. Dormieux, D. Kondo, F. Ulm, Microporomechanics, Wiley & Sons, 2006.

[39] P. A. Lock, X. D. Jing, R. W. Zimmerman, E. M. Schlueter, Predicting the permeability of sandstone from image analysis of pore structure, J. Appl. Phys. 92 (2002) 6311–6319.

[40] M. Kachanov, Effective elastic properties of cracked solids: critical review of som basic concepts, Appl. Mech. Rev. 45 (8) (1992) 304–335.

[41] M. Ortiz, A constitutive theory for the inelastic behaviour of concrete, Mech. Mater. 4 (1985) 67–93.

[42] R. AbuAlRub, G. Voyiadjis, On the coupling of anisotropic damage and plasticity models for ductile materials, Int. J. Solids A/ Struct. 40 (2003) 2611–2643.

[43] A. Chiarelli, J. Shao, Modélisation élastoplastique couplée à l'endommagement anisotrope induit pour les argilites, Revue Française de Génie Civil 6 (1) (2002) 115–130.

[44] F. Homand-Etienne, D. Hoxha, J. Shao, A continuum damage constitutive law for brittle rocks, Computers and Geotechnics 22 (2) (1998) 135–151.

[45] G. Swoboda, Q. Yang, An energy-based damage model of geomaterials 1. formulation and numerical reults, Int. J. Solids and Struct. 36 (1999a) 1719–1734.

[46] J. Cordebois, F. Sidoroff, Endommagement anisotrope en élasticité et plasticité, Journal de Mécanique théorique et appliquée (special issue) (1982) 45–60.

[47] J. Chaboche, Development of continuum damage mechanics for elastic solids sustaining anisotropic and unilateral damage, International Journal of Damage Mechanics 2 (1993) 311–329.

[48] D. Ronen, H. Scher, M. Blunt, On the structure and flow processes in the capillary fringe of phreatic aquifers, Transport in Porous Media 28 (1997) 159–180.

[49] D. Ronen, H. Scher, M. Blunt, Field observations of a capillary fringe before and after a rainy season, Journal of Contaminant Hydrology 44 (2000) 103–118.

[50] M. Blunt, Flow in porous media - pore-network models and multiphase flow, Current Opinion in Colloid & Interface Science 6 (2001) 197–207.

[51] P. Delage, Y.-J. Cui, L'eau dans les sols non saturés, Techniques de l'Ingénieur (C301) (2000) 1–20.

[52] R. Craig, Craig's Soil Mechanics, Seventh Edition, Spon Press, 2004, Ch. 1, pp. 1–29.

[53] O. Coussy, Mechanics and Physics of Porous Solids, Wiley & Sons, 2010.

[54] T. Lacy, D. MacDowel, R. Talreja, Gradient concepts for evolution of damage, Mechanics of Materials 31 (1999) 831–860.

[55] F. Homand, A. Chiarelli, D. Hoxha, Caractéristiques physiques et mécaniques du granite de la vienne et de l'argilite de l'est, Revue Française de Génie Civil 6 (1) (2002) 11–20.

[56] C. Arson, B. Gatmiri, Numerical study of a thermo-hydro-mechanical damage model for unsaturated porous media, Annals of Solid and Structural Mechanics 1 (2010) 59–78.

[57] D. Halm, A. Dragon, Modélisation de l'endommagement par mésofissuration du granite, Revue Française de Génie Civil 17 (2002) 21–33.

[58] J. Kozeny, Ueber turbulentes fliessen bei glatten waenden., Ztschr. angew. Math. und Mech. 5 (1925) 244–250.

[59] P. Carman, Fluid flow through granular beds, Transactions - Institution of Chemical Engineers 15 (1937) 150–166.